An Experimental Study of Natural Gas Jet-flames in Crossflow with High Hydrogen Admixture at Elevated Pressure Conditions

I. Boxx[1,*], J. Pareja[1], P. Saini[1]
1: Institut für Verbrennungstechnik, Deutsches Zentrum für Luft-und Raumfahrt, Germany
* Correspondent author: Isaac.Boxx@dlr.de

Keywords: Jet flame in crossflow, PIV, dual-plane PLIF

ABSTRACT

A series of high hydrogen-content jet flames in crossflow are investigated experimentally using high-speed (10 kHz) stereoscopic particle image velocimetry, dual-plane laser-induced fluorescence of the hydroxyl radical, and OH* chemiluminescence imaging. The flames were fueled with natural gas enriched to 70-, 80-, 90- and 100% H_2, by volume at conditions approaching those found in the mixing duct of a modern gas turbine engine, specifically in close confinement, at 7 bars pressure and with a crossflow preheat of 511 K.

Consistent with (Hasselbrink and Mungal, 1998), the measurements indicate the recirculation zone on the leeward side of the jet plays a critical role in stabilization of the lifted jet flame in crossflow. The measurements show that local heat-release from a flame in this region acts as a self-reinforcing feedback mechanism, strengthening the recirculation zone and increasing local residence time there. This, in turn, creates conditions more favorable to flame stabilization. The measurements also showed how close confinement of the JICF by the flow channel walls affects jet-penetration and growth of the counter-rotating vortex pair.

1. Introduction

In gas turbines, fuel is often introduced to the combustor as a jet-in-crossflow (JICF). To ensure uniform fuel-air mixing prior to combustion, there is usually a mixing channel between the fuel injector and the combustion chamber. A particularly destructive failure mode for gas turbine combustors occurs when the flame propagates upstream of the combustor and anchors in the mixing channel. With increasing consideration of hydrogen (which has a much higher flame speed than natural gas) as a carbon-free fuel for gas turbines, a fuller understanding the dynamics of flame holding and stabilization in confined, hydrogen-rich reacting JICF is essential.

The jet-in-crossflow is a widely studied, canonical flow configuration. Its flowfield is characterized by a set of four strongly interacting vortex systems: a counter-rotating vortex pair (CVP), shear-layer vortices, horseshoe vortices, and wake vortices (Margason 1993; Mahesh 2013; Schlüter and Schönfeld 2000; Kelso et al. 1996; Fric and Roshko 1994; Smith and Mungal 1998). The CVP, which

forms in the core of the jet, dominates the far-field of the JICF. The shear layer vortices form as a result of the Kelvin-Helmholtz instability induced by the shear-layer between the jet and the crossflow. The horseshoe vortex forms in the crossflow upstream of JICF and (as its name implies) takes on a horseshoe shape as it passes around the jet. The wake vortices originate in the boundary layer of the wall and form downstream of the jet exit orifice (Karagozian 2010).

The stabilization mechanism responsible for flame-holding in reacting JICF has been the focus of much research in recent years (Hasselbrink and Mungal, 1998; Chen 2011; Grout et al. 2011, 2012; Kolla et al. 2012; Steinberg et al. 2013; Chan et al. 2014). These studies have noted that a recirculation zone on the leeward side of the JICF is critical to flame stabilization. The effect of various combustor design parameters such as jet density, flame speed and combustor pressure on this stabilization mechanism have, however, yet to be fully explored.

The goal of this study was to explore the mechanism responsible for stabilization and anchoring of turbulent, non-premixed high hydrogen-content jet-flames in crossflow at conditions representative of a modern gas combustor. We accomplish this by performing high-speed stereoscopic particle image velocimetry (SPIV), dual-plane laser induced fluorescence of the hydroxyl radical (OH-PLIF), and OH* chemiluminescence (OH* CL) imaging on a series of turbulent, non-premixed reacting- and nonreacting JICF with hydrogen fuel-fractions (HFF) ranging from 70- to 100% (by volume). Combustor pressure and temperature, crossflow velocity and jet-to-crossflow momentum ratio were held constant across the four test cases. We analyze these measurements to identify the dominant parameters responsible for flame stabilization and anchoring, and explore how confinement of the jet by the flow-channel walls affects jet penetration and growth of the counter-rotating vortex pair.

2. Experimental Setup

2.1 - Jet in Crossflow Facility

The experiments described in this paper were performed in the test facility described in our previous studies (Saini et al., 2020, 2021). For completeness, a brief description is provided below. The JICF facility consisted of a flow channel and fuel injector (Fig. 1) housed in a high pressure, optically accessible combustion vessel. The flow channel was modular in design, with each of the three modules having a rectangular cross-section (measuring 40 × 60 mm). The fuel injector was mounted in the third (i.e. the most downstream) of these modules. The purpose of having two modules of the flow channel upstream of the injector was to ensure a well-developed turbulent boundary layer formed along the plate upstream of the jet-exit. Upstream of the first module was a settling chamber with a flow conditioning screen and an inlet for the injection of air seeded with

tracer particles (necessary for the SPIV measurements).

The non-premixed fuel jet issued from a 2 mm diameter circular orifice mounted flush with the lower (40 mm wide) wall of the flow channel. Beneath the orifice was a nozzle designed to produce a uniform, top-hat velocity profile at the jet-exit. The nozzle has fifth order polynomial profile and has been shown in previous studies (Megerian, et al. 2007) to produce a uniform, top-hat velocity profile at the jet exit. A flow conditioning screen at the base of the injector nozzle ensures a stable, symmetric flow throughout. The nozzle block is water-cooled to ensure constant fuel temperature.

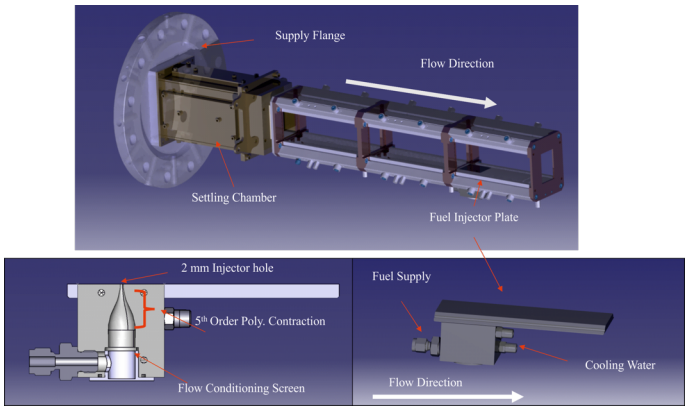

Figure 1 - Jet-in-crossflow facility (upper), and fuel-injector nozzle (bottom)

2.2 - Laser Diagnostic Systems

Three high-bandwidth, kHz acquisition-rate laser diagnostic measurement systems were implemented in this study: stereoscopic particle image velocimetry, OH* chemiluminescence imaging, and dual-plane laser-induced fluorescence of the hydroxyl radical (dual-plane OH-PLIF). In contrast with our earlier studies, each diagnostic was deployed separately in this study, rather than synchronously, to enable better optimization of each system. The orientation of the laser-imaging systems with respect to the JICF facility are shown schematically in Fig. 2. Elements of this system have been described in previous papers but for completeness, are presented again below.

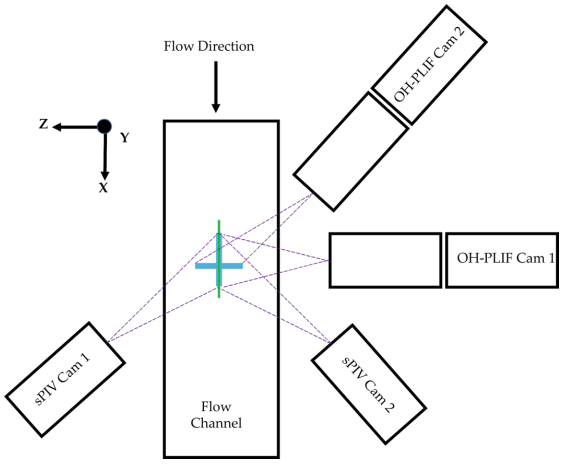

Figure 2 - Orientation of the laser measurement systems, with respect to the JICF facility.

2.2.1 SPIV

The SPIV system consisted of a dual-cavity, diode-pumped, solid-state, frequency-doubled Nd:YAG laser (Edgewave, IS200-2-LD) and a pair of high-speed CMOS cameras (Phantom V1212). The laser and cameras were synchronized to run at a cyclic repetition rate of 10 kHz. The laser emitted pairs of pulses, with energies of up to 9mJ ea., that were used to illuminate TiO_2 particles (≈1 μm in size) seeded into the jet and crossflow. The laser sheet measured approximately 40 mm (wide) × 1 mm (thick) at the measurement region.

The CMOS cameras were equipped with 200-mm focal-length, f/4 macro objective lenses (Nikon AF-Micro Nikkor) and 532-nm-bandpass interference filters to suppress background flame luminosity. Off-axis imaging blur was mitigated through the use of Scheimpflug adapters. The cameras were operated in dual-frame mode with an image resolution of 896 × 656 pixels, which resulted in a field of view of 54 × 40 mm (in the axial and transverse directions, respectively).

Velocity vectors were calculated using a multi-pass adaptive window offset cross-correlation function via a commercially available software package (LaVision Davis 10.2.0). The final interrogation window size and overlap were 16 × 16 pixels and 50%, respectively. This yielded a spatial resolution of 0.97 mm/vector and vector spacing of 0.484 mm.

2.2.2 Dual-Plane OH PLIF

The dual-plane OH-PLIF system consisted of two identical lasers and imaging systems, coupled together via beam combining optics. Each system used an intensified CMOS camera system, a frequency-doubled, Q-switched, diode-pumped solid state Nd:YAG laser (Edgewave IS400-2-L supplying 110 W at 532 nm), and a frequency-doubled dye laser that was pumped by the aforementioned YAG laser. The dye laser systems (Sirah Credo) each produced 5 W at 283.9 nm and had a pulse-repetition frequency of 10 kHz. The lasers were both tuned to excite the (closely spaced) Q1(9) and Q2(8) lines within the $A^2\Sigma^+ - X^2\Pi\ (v' = 1, v' = 0)$ band. The wavelength was

monitored by directing a small percentage of each laser beam through a laminar reference flame and monitoring the resulting signal using a photomultiplier tube and a digital oscilloscope.
The OH-PLIF laser sheets were approximately 40 mm (wide) × 0.2 mm (thick), and overlapped by rotating the polarization of one beam with a half wave plate and reflecting it from the front surface of a thin film polarizer through which the second beam passed from behind. Fluorescence signal was acquired with a pair of CMOS cameras (LaVision HSS8) equipped with external two stage lens-coupled intensifiers (LaVision HS-IRO). The camera aligned with the OH-PLIF laser on the axial centerline of the flow channel was equipped with a 64-mm focal length, f/2 UV lens (Halle Nachfl.). The second camera, aligned with the cross-plane PLIF sheet, was equipped with a 100mm focal length, f/2.8 (Cerco) objective. Elastic scattering (at 283 nm) was blocked with the use of a high-transmission (> 80% at 310 nm) bandpass filter while background flame emission was further limited with a 100-ns intensifier gate. To ensure optical access across the full width of the flow channel, the two laser sheets were aligned to intersect 24mm downstream of the fuel injector.

2.2.3 OH* CL

The intensified camera of the OH-PLIF measurement system aligned with the axial centerline of the flow channel was employed to (separately) record OH* chemiluminescence from the flames. OH* chemiluminescence is a robust (line-of-sight integrated) marker for combustion heat release. The integration time for the OH*-CL signal was 25 μs.

2.3 Test Conditions

Four non-premixed JFICF were studied in this project. The fluid-dynamic and chemical parameters for each case are summarized in Table 1. These cases correspond to natural gas jet flames enriched to 70-, 80-, 90- and 100% H_2, by volume. In order to isolate the effect of hydrogen on flame dynamics, we hold constant key parameters of the JFICF for each case, while varying the H_2 levels. The parameters held constant were the crossflow temperature and velocity (511 K and 10 m/s, respectively), chamber pressure (7 bars), and the jet-to-crossflow momentum flux ratio (r = 6).
The crossflow temperature was set so as to mimic the temperature of air undergoing adiabatic compression (e.g. through the compressor of a gas turbine engine) from 1 bar (atmospheric) to 7 bars pressure. The natural gas used in this study consisted of approximately 94% CH_4, 4% C_2H_6 and 2% other gases (N_2, CO_2, CO and higher hydrocarbons), by volume. The density of the fuel mixtures was calculated using a mole-weighted sum of the densities of the constituent gases of the mixtures.

Table 1 – Run Conditions

Condition	Pressure (Bars)	J	U_{cf} (m/s)	% Vol. H_2
1	7	6	10	70%
2	7	6	10	80%
3	7	6	10	90%
4	7	6	10	100%

3 - Results and Discussion

Figure 3 shows sample OH-PLIF measurements acquired in the JICF with 100% (upper row) and 70% (lower row) HFF. The red lines indicate where the two OH-PLIF laser sheets Intersect.

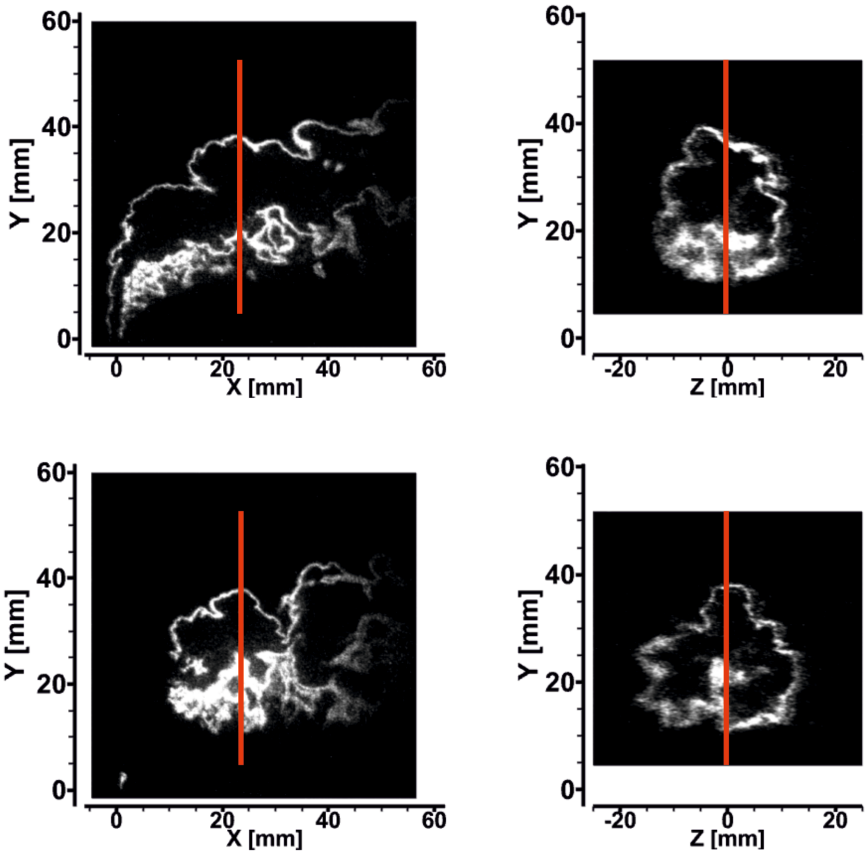

Figure 3 - Sample OH-PLIF measurements in axial (left) and cross (right) plane direction. The upper row shows the flame with 100% HFF, and the lower 70% HFF.

Figure 3 illustrates several important features of the JICF test cases. The OH-PLIF image aligned with the axial centerline of the burner shows the case with 100% HFF has an intact flame front along both the windward- and leeward side of the jet, and is nozzle-attached. The flame on the windward side of the jet is thin and appears to conform to the shear-layer. The flame on the leeward side is much more diffuse and wrinkled. The JICF with 70% HFF, shows flame-extinction along both the windward- and leeward side of the jet, and appears to stabilize as a lifted flame in the crossflow. The OH-PLIF measurement acquired in the cross plane for each case shows (at least for this instant in time) an intact flame front around the periphery of the jet.

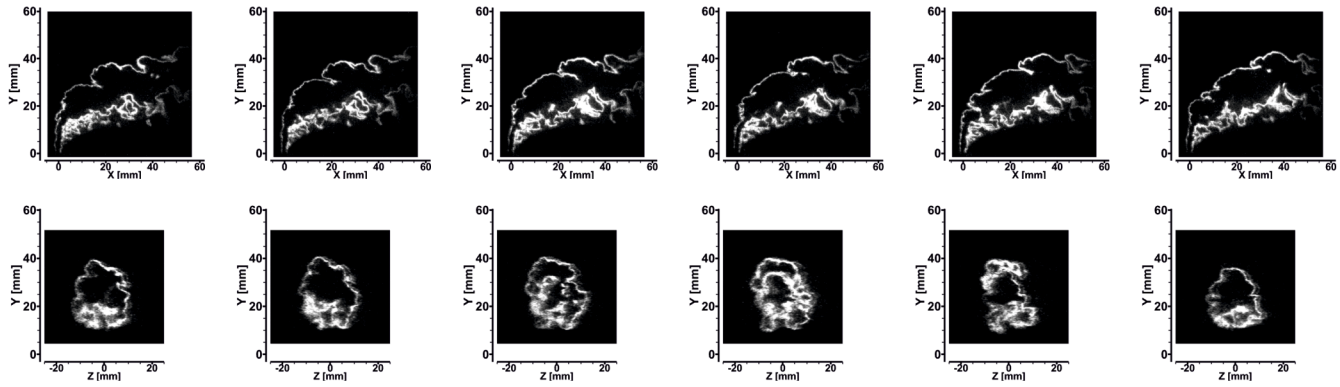

Fig. 4 Sample dual-plane OH-PLIF measurement sequence of the JICF with 100% HFF. Every second measurement is shown, corresponding to a frame-to-frame time difference of t = 0.2 ms.

Figure 4 shows a sample measurement sequence acquired with the dual-plane OH-PLIF system in the JICF with 100% HFF. For clarity, only every second frame is displayed. In this image sequence, we see that the flame on the windward side of the jet is thin, intact and appears to conform to the shear-layer vortices. In conforming to the shear layer vortices, the flame is seen to roll-up and "fold" in upon itself with increasing downstream distance. This leads to occasional flame-flame interaction and entrainment of hot combustion products into the high velocity core of the jet. An example of such a roll-up and burnout is visible from the first frame onward, at approximately 30 mm above the injector wall. The flame on the leeward side of the jet is much more diffuse and wrinkled. The scale of the flame wrinkles on the leeward side grows with downstream distance and by approximately 40 mm downstream, begin to resemble the large-scale roll-up and "folding" observed on the windward side. This suggests that, whereas the near-field flame dynamics on the windward are driven by different mechanisms on the windward and leeward side, flame dynamics in the far-field are dominated on both sides by the shear-layer vortices.

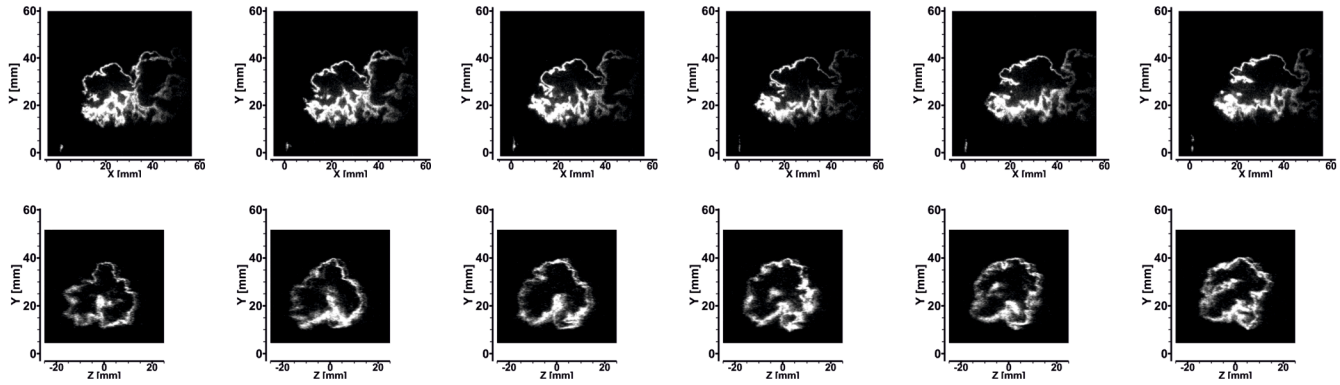

Fig. 5 Sample dual-plane OH-PLIF measurement sequence of the JICF with 70% HFF. Every second measurement is shown, corresponding to a frame-to-frame time difference of t = 0.2 ms.

Figure 5 shows a sample measurement sequence acquired with the dual-plane OH-PLIF system in the JICF with 70% HFF. In all images acquired in the plane aligned with the jet centerline, a small pocket of flame is visible at the flow channel wall, immediately behind the jet-exit. The rest of the flame appears detached and burns as a lifted jet flame in the heated crossflow. Given that OH-PLIF is a planar measurement technique, one cannot discount the possibility of there being a contiguous flame front between the wall and the "lifted" part of the flame outside of the centerline imaging plane. Important to note though, is that the flame is clearly not fully attached in the near-field of the jet. The cross-plane OH-PLIF measurements in Fig. 5 indicate that at axial distance of 24 mm downstream of the injector, a largely contiguous flame sheet surrounds the periphery of the jet.

Stabilization Mechanism

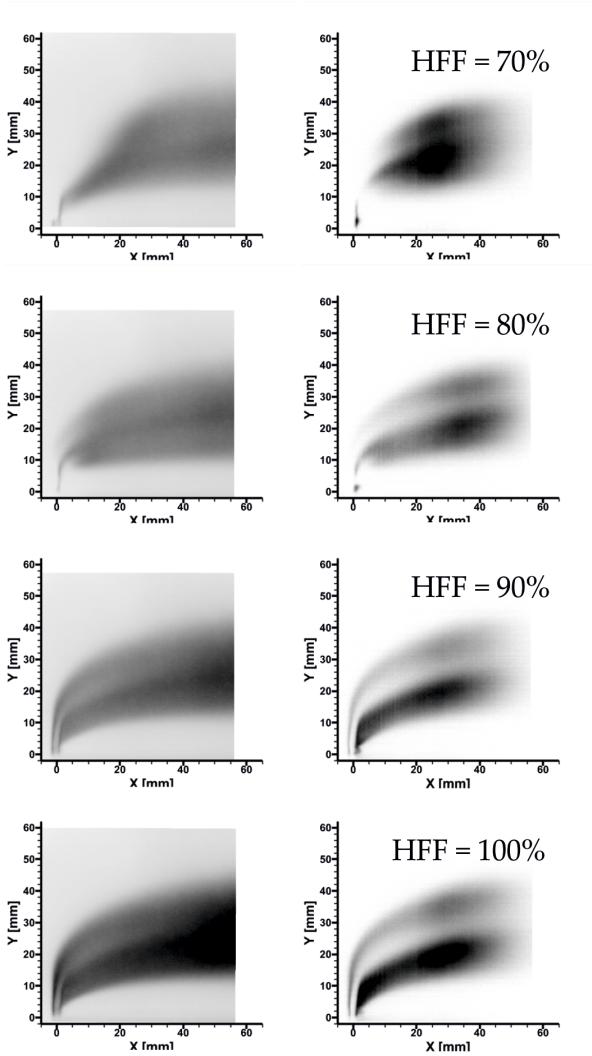

Fig. 6 Mean OH* Chemiluminescence (left) and OH-PLIF (right) measured for each test case.

Figure 6 shows the ensemble-averaged OH* chemiluminescence and OH-PLIF measurements for each test case. The flames with 90- and 100% HFF both appear to be fully nozzle-attached, with intact flames along the windward side of the jet. Consistent with previous studies, they also show considerably wider and more diffuse heat-release zones on the leeward side of the jet than on the windward side. This well-known asymmetry results from intense fuel-air mixing and increased residence times associated with the counter-rotating vortex core.

The flames with 70- and 80% HFF are seen to be extinguished on the windward side of the jet, and burn as lifted flames in the crossflow. The mean OH-PLIF image for the flame with 70% HFF shows a small pocket of flame at the wall immediately behind the injector nozzle exit (i.e. at axial location $x \approx 1$ - 2 mm). The mean OH* chemiluminescence image shows a thin band of heat-release connecting this flame pocket and the main lifted flame. The flame with 80% HFF shows a similar overall structure, albeit with a stronger connection between the wake-stabilized flame pocket at the wall and the (lifted) main flame.

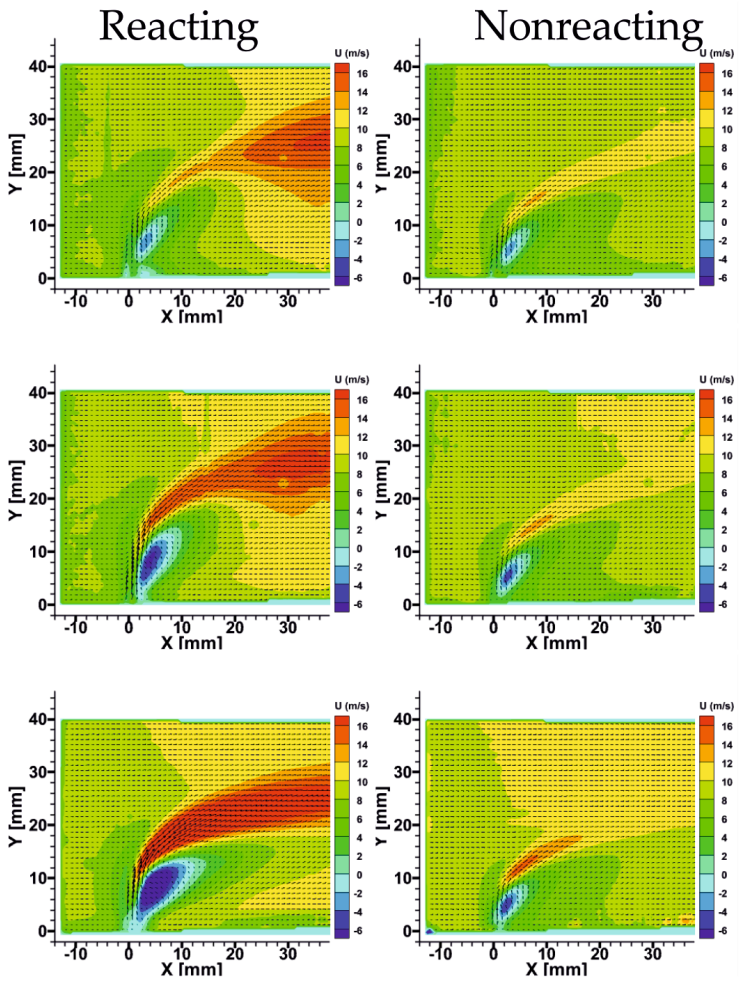

Fig. 7 Mean axial velocity for reacting (left) and non-reacting (right) measured in JICF with HFF = 70% (top), 80% (middle) and 100% (bottom).

To better understand the effect of this flame pocket on the lifted JFICF, Fig. 7 shows the mean axial velocity measured in the JICF with 70-, 80- and 100% HFF. We note that the limited spatial resolution (0.97 mm/vector) of the SPIV system, together with very high seed density at the jet-exit made it impossible to accurately capture the high velocity flow along the jet centerline in the near-field ($0 < s/rd < \approx 2$). As such, the colorbars are adjusted to highlight the (accurately measured) lower velocity crossflow, wake and downstream regions of the jet centerline flow ($s/rd > 2$).

The ensemble-averaged fields of axial velocity plotted in Fig. 7 reveal the presence of a recirculation zone on the leeward side of each (reacting and nonreacting) JICF. These appear as blue in the color scheme of the figure, and persist all the way to the flow channel wall, where they overlap the location of the flame-pockets identified in Fig. 6. The existence of a recirculation zone in the near-field wake of a JICF is well established in the scientific literature (Kelso et al., 1996;

Cortelezzi and Karagozian, 2000; Lim et al. 2001), and is associated with the formation of the CVP. Previous studies (Hasselbrink and Mungal, 1998; Han and Mungal, 2002) have concluded that the recirculation zone on the leeward side of the a piloted JICF plays an important role in stabilization of a lifted jet flame in crossflow. The effect of various combustor design parameters such as jet density, flame speed and combustor pressure on this stabilization mechanism have, however, yet to be fully explored.

Figure 7 shows that the size and strength of the recirculation zones grow significantly with increasing hydrogen concentration in the reacting flow cases, despite maintaining a constant momentum flux ratio. The recirculation zones of the non-reacting JICF are much less sensitive to HFF in the jet. In addition, the recirculation zones of the reacting JICF are significantly larger and stronger than those of the non-reacting. This suggests local heat-release from the flame, more than jet-exit velocity or density, is the dominant parameter affecting the recirculation zone in reacting JICF. Hydrogen has a higher adiabatic flame temperature, laminar flame speed and extinction strain rate than methane. This would result in more stable flame anchoring and a higher heat-release rate in the recirculation zone, and may explain why the reacting JICF are more affected by hydrogen-enrichment than the non-reacting cases.

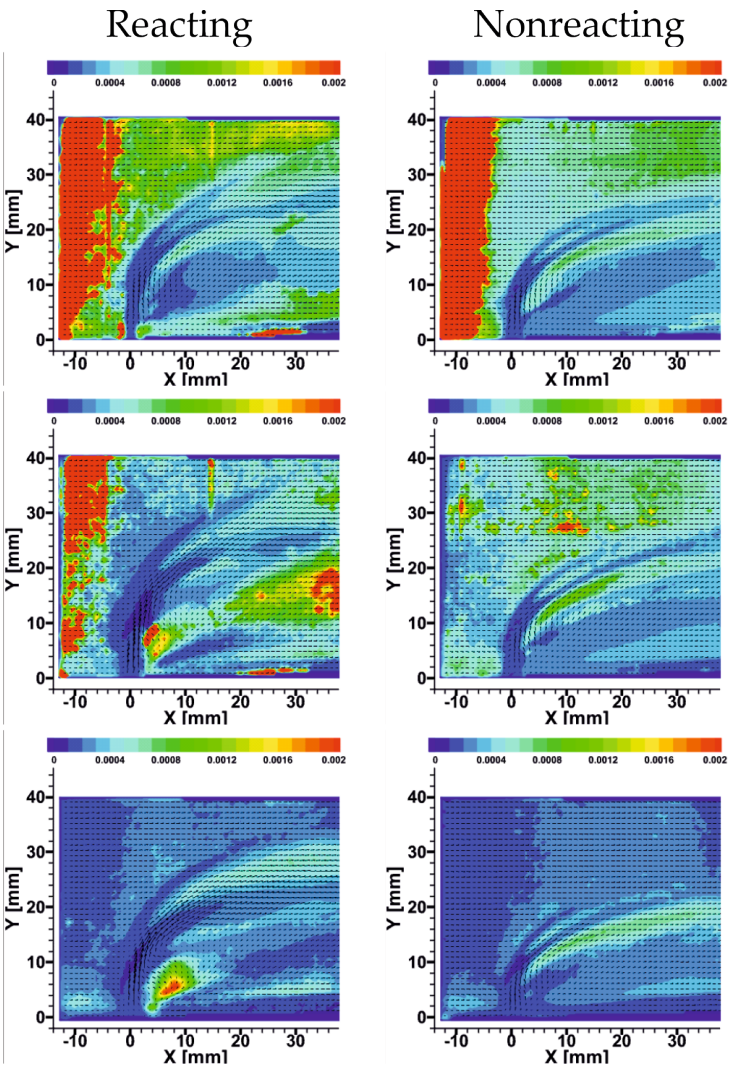

Figure 8 - Integral timescale in axial direction for reacting (left) and non-reacting (right) JICF with HFF = 70% (top), 80% (middle) and 100% (bottom). Colorbars are shown in units of seconds.

To explore the effect of the recirculation zones identified in Fig. 7 on residence times of the reactant mixture, the time-resolved SPIV measurements were used to compute integral timescales at each vector location. The results are shown in Fig. 8. As expected, one observes significantly greater integral timescales in the leeward-side recirculation zone than elsewhere in the flow. Consistent with our observations of Fig. 7, this increase is only observed in the reacting flow cases. This supports the conclusion that local heat-release from the flame pockets identified in Fig. 6 is a key parameter affecting the size and strength of these recirculation zones. The presence of a flame in the leeward side recirculation zone appears to act as a feedback mechanism. Its heat-release strengthens the recirculation zone and increases local residence time, both of which are favorable to mixing and flame stabilization.

Confinement Effects

Figure 6 hints at the existence of a significant jet-confinement effect in this burner. Previous studies (Hasselbrink and Mungal, 2001) have shown that the presence of an intact flame at the periphery of a JICF acts to impede crossflow entrainment and thereby leads to greater penetration of reacting jets in crossflow compared to non-reacting ones. Consistent with our previous studies (Saini et al., 2020, 2021) however, we do not observe such a difference. Rather, we observe similar penetration and jet-spreading (in the transverse direction) for all four test conditions, despite the clear differences in global flame structure.

A plausible explanation for the similarity in jet penetration across the four test conditions (despite clear differences in the windward side flame structure) is that confinement of the JICF by the flow channel is acting to impede or limit the entrainment of crossflow. Given that entrainment in the JICF occurs at the shear-layer between the high velocity jet and the lower velocity co-flow, once the jet reaches a size similar to that of the flow channel, the shear-layer (and the surrounding crossflow) disappears and entrainment will cease. Looking at Fig. 6, we see that the flame does not impinge significantly on the upper wall of the flow channel (at y = 60 mm) within the first 50 mm downstream of the jet-exit. It does, however, grow to a width (in the transverse direction) of approximately 35 mm, extending from y ≈ 10 to 45 mm. Recall that the flow channel measures 40 × 60 mm in the z- and y-directions, respectively. Given the geometry of the CRT, an unconfined JICF expands significantly faster with downstream distance in the Y-Z plane than it does in the X-Y plane. It is therefore reasonable to assume confinement effects by the flow-channel walls (at z = +/- 20mm) are significant.

To look for evidence of jet-confinement effects in the through-plane direction, we now examine the ensemble-averaged OH-PLIF measurements acquired with the crossplane OH-PLIF system. Fig. 9 shows the ensemble-averaged OH-PLIF signal measured perpendicular to the axial flow direction for Test Conditions 1 and 4, with increasing downstream distance. The first frame corresponds to the plane 24 mm downstream of the jet-exit, and each subsequent row represents an additional 20 mm downstream displacement.

Figure 9 shows (as expected) the dominant flow structure in the Y-Z plane is the CVP. In the measurements acquired at x = 24 mm (top row), both JICF have an approximately circular shape, with a diameter of approximately 30 mm. The OH-PLIF signal is found mainly along the outer periphery of the CVP, and extends deep into the core of the jet. In the 70% HFF case, OH signal peaks in the upper half of the JICF, well above the centers of rotation for each side-lobe of the CVP. In the 100% HFF flame, OH signal is observed mainly along the periphery of the CVP. The difference in OH distribution for these two cases is consistent with the 70% HFF case having

greater penetration and mixing of the heated crossflow along the windward side of the jet. This suggests that confinement effects are not dominant at this axial location.

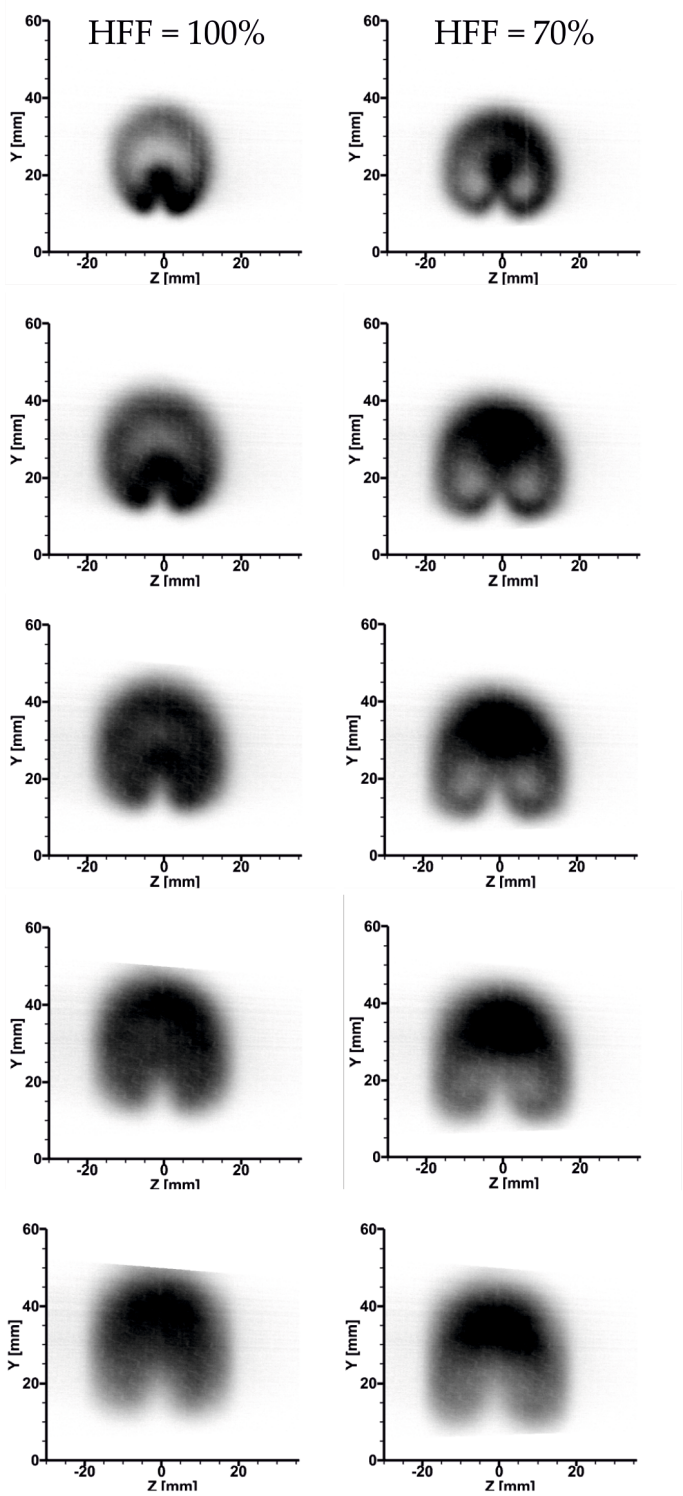

Fig. 9 Mean OH-PLIF measured in the cross-plane direction for JICF with 100% (left) and 70% (right) HFF. The top row corresponds to x = 24 mm, and each subsequent row represents a further displacement of 20 mm downstream

At x = 44 mm, in the second row of Fig. 9, we observe the diameter of the JICF has increased and moved further from the injector wall, but is otherwise similar to that measured at x = 24mm. By x = 64 mm, the effect of confinement by the side-walls of flow channel becomes apparent. The side-lobes of the CVP begin to appear elongated in the vertical direction, rather than continuing to expand in the +/- z-direction. This is clearly linked confinement by the side-walls of the flow-channel, which are found at z = +/- 20 mm. This effect becomes more obvious with increasing downstream distance. This confinement of the JICF by the flow-channel side walls will significantly impede crossflow entrainment at the sides of the jet and may explain the similarity of jet penetration across the four test cases.

4. Conclusions

A series of jet flames in crossflow were investigated experimentally using high-speed (10 kHz) stereoscopic particle image velocimetry, dual-plane laser-induced fluorescence of the hydroxyl radical, and OH* chemiluminescence imaging. The flames were fuelled with natural gas enriched to 70-, 80-, 90- and 100% H_2, by volume at conditions approaching those found in the mixing duct of a modern gas turbine engine.

Consistent with the findings Hasselbrink and Mungal (1998), the measurements show the recirculation zone on the leeward side of the jet plays a critical role in stabilization of the lifted jet flame in crossflow. They show that local heat-release from the flame in this region acts as a self-reinforcing feedback mechanism, strengthening the recirculation zone and increasing local residence time there and, in the process, creating conditions favourable to flame stabilization. This finding has significant implications for understanding ignition and flame-holding in fuel injectors based on the JICF. The measurements also showed how close confinement of the JICF by the flow channel walls affects jet-penetration and growth of the CVP.

Acknowledgements

This project has received funding from the European Research Council (ERC) under the European Union's Horizon 2020 research and innovation programme (Grant Agreement No. 682383).

References

Chan, W.L., Kolla, H., Chen, J.H., Ihme, M.: Assessment of model assumptions and budget terms of the unsteady flamelet equations for a turbulent reacting jet-in-cross-flow. Combust. Flame 161(10), 2601– 2613 (2014)

Chen, J.H.: Petascale direct numerical simulation of turbulent combustion-fundamental insights towards predictive models. Proc. Combust. Inst. 33(1), 99–123 (2011).

Cortelezzi, L., Karagozian, A.R.: On the formation of the counter-rotating vortex pair in transverse jets. J. Fluid Mech. 446, 347–373 (2001)

Fric, T.F., Roshko, A.: Vortical structure in the wake of a transverse jet. J. Fluid Mech. 279, 1–47 (1994).

Grout, R.W., Gruber, A., Yoo, C.S., Chen, J.H.: Direct numerical simulation of flame stabilization downstream of a transverse fuel jet in cross-flow. Proc. Combust. Inst. 33(1), 1629–1637 (2011).

Han, D., Mungal, M.G.: Stabilization in turbulent lifted deflected-jet flame. Proc. Combust. Inst. 29, 1889–1895, (2002).

Hasselbrink, E.F., Mungal, M.G.: Transverse jets and jet flames. part 1. scaling laws for strong transverse jets. J. Fluid Mech. 443, 1–25 (2001a).

Karagozian, A.R.: Transverse jets and their control. Prog. Energy Combust. Sci. 36(5), 531–553 (2010).

Kelso, R.M., Lim, T.T., Perry, A.E.: An experimental study of round jets in cross-flow. J. Fluid Mech. 306, 111–144 (1996).

Kolla, H., Grout, R.W., Gruber, A., Chen, J.H.: Mechanisms of flame stabilization and blowout in a reacting turbulent hydrogen jet in cross-flow. Combust. Flame 159(8), 2755–2766 (2012).

Lim, T.T., New, T.H., Luo, S.C.: On the development of large-scale structures of a jet normal to a cross flow. Phys. Fluids. 13, 770 (2001).

Mahesh, K.: The interaction of jets with crossflow. Annu. Rev. Fluid Mech. 45, 379–407 (2013).

Margason, R.J.: Fifty years of jet in cross flow research, symposium, computational and experimental assessment of jets in cross flow. In: Computational and experimental assessment of jets in cross flow, Agard Conference Proceedings Agard CP, Symposium, Computational and experimental assessment of jets in cross flow, number 534, pp. 1–2. NATO, (1993). ISBN 9283507207.

Megerian, S., Davitian, J., de B Alves, L.S., Karagozian, A.R.: Transverse-jet shear-layer instabilities. part 1. experimental studies. J. Fluid Mech. 593, 93–129 (2007).

Saini, P., Chterev, I., Pareja, J., Aigner, M., Boxx, I.: Effect of Pressure on Hydrogen Enriched Natural Gas Jet Flames in Crossflow. Flow Turbul. Combust. 105, 787–806 (2020).

Saini, P., Chterev, I., Pareja, J., Aigner, M., Boxx, I.: Effects of Hydrogen-Enrichment on Flame-Holding of Natural Gas Jet Flames in Crossflow at Elevated Temperature and Pressure. Flow Turbul. Combust. 107, 219–243 (2021).

Schlüter, J.U., Schönfeld, T.: Les of jets in cross flow and its application to a gas turbine burner. Flow Turbul. Combust. 65(2), 177 (2000).

Smith, S.H., Mungal, M.G.: Mixing, structure and scaling of the jet in crossflow. J. Fluid Mech. 357, 83–122 (1998).

Steinberg, A.M., Sadanandan, R., Dem, C., Kutne, P., Meier, W.: Structure and stabilization of hydrogen jet flames in cross-flows. Proc. Combust. Inst. 34(1), 1499–1507 (2013).